Preprints of the 21st IFAC World Congress (Virtual)
Berlin, Germany, July 12-17, 2020

Approximate Time-Optimal Control Considering System Bandwidth and Saturation ⋆

Yunjie Yang * **Yang He** *,** **Jihong Zhu** ***

* *Department of Computer Science and Technology, Tsinghua University, Beijing, China, (e-mail: yyj15@mails.tsinghua.edu.cn)*
** *School of Electrical and Information Engineering, Jiangsu University, Zhenjiang, China, (e-mail: heyang@tsinghua.edu.cn)*
*** *Department of Precision Instrument, Tsinghua University, Beijing, China, (e-mail: Jihong_Zhu@hotmail.com)*

Abstract: Time-optimal (TO) control is promising in many fields since it ensures to accomplish a task in minimum time. However, its direct application may cause oscillations or even limit cycles due to the restriction of the sampling period, state measurement accuracy and so on. To solve these problems, a compound proximate time-optimal (PTO) control law is proposed by considering system bandwidth and saturation in this paper. With the help of the phase plane, the switching zone and linear zone of the PTO control law are constructed. When the system state lies outside of both switching and linear zones, the bang-bang optimal scheme is adopted to achieve rapidity. And when the system state enters the switching zone, the bang-bang suboptimal scheme is developed to avoid oscillations or even limit cycles. Proportional-derivative (PD) scheme is applied in the linear zone to obtain local asymptotic stability around the origin. Numerical simulations are carried out to corroborate the advantages of the PTO control law.

Keywords: Proximate time-optimal, Minimum principle, Bang-bang scheme, Switching zone

1. INTRODUCTION

Optimal control is a well developed method which aims to optimize a specific performance index (Bryson (2018)). Among various forms of optimal criteria, time-optimal (TO) is a promising one in many fields like mechanical arms (Herlant et al. (2016)), servo systems (Lu and Shieh (2014); HU et al. (2018)) and so on. The target of time-optimal control (TOC) is to transfer the system from an initial state to a desired state as quick as possible.

Since the control input is bounded generally, the solution of TOC forms as a bang-bang scheme, which means the control input constantly switching between its minimum and maximum values (Bonifacius et al. (2019)). The basic utilization of TOC is in a dual integrators system, where the switching curve is a simple quadratic parabola (Rao and Bernstein (2001); Grimholt and Skogestad (2016)). However, its direct application to practical systems is not feasible due to the restriction of the sampling period, state measurement accuracy and so on. Oscillations or even limit cycles are possible to occur, which are undesirable (Dhanda and Franklin (2009)). Adaptive proximate time optimal servomechanism (PTOS) developed by Workman et al. (1987a,b) is a widely used technique in addressing this problem. By replacing the sign function as the saturation function, a region to avoid chattering problems was formed. Besides, when the system state approaches the given target, the linear control is adopted. With these two strategies, the robustness of the system is strengthened, but this is at the expense of decreased dynamic performance. Choi et al. (2006) proposed a damping scheduling PTOS (DSPTOS), which keeps the damping coefficient of the closed-loop system at a predetermined value. Therefore, by setting different damping in the deceleration phase and settling phase, it is able to speed up the system dynamic response while ensuring a smaller overshoot and weaker residual vibrations. A PTOS$\omega\zeta$ tracking controller was developed for a damped harmonic oscillator. But its complexity requires a lookup table for the implementation, which weakens the robustness of the controller in the application (Braker and Pao (2017)).

Considering the fact that in many rigid systems, the bandwidth and saturation limits make the command velocity hard to be tracked instantaneously. As shown in Fig. 1, under an inner loop controller, the velocity loop generally features as the first-order system (Featherstone (2014)). The velocity saturation and the bandwidth are the two important factors. Thus the PTOS and its various improvements on the double integrator system cannot be directly used. Park and Won (1991) derived the TOC switching curve, but the possible oscillations caused by inaccurately switch in practical systems are not considered.

In this paper, a compound proximate time-optimal control (PTO) method is designed for these rigid body systems. According to the minimum principle (Bertsekas (1995)),

⋆ This work was supported in part by National Natural Science Foundation of China (Grant Nos. 61603210 and 61973182) and in part by Aeronautical Science Foundation of China (Grant No. 20160758001).

Copyright lies with the authors

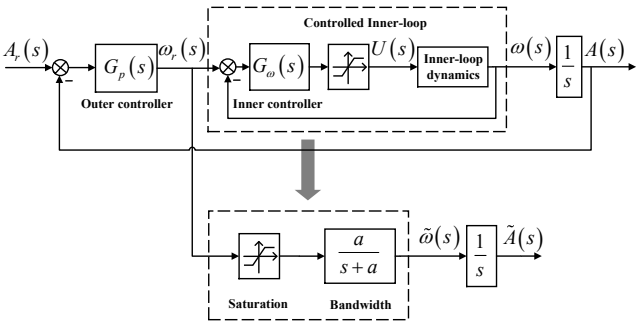

Fig. 1. Dynamics of rigid body systems

the switching curve becomes a complex logarithmic function. Since the sampled discrete system states are hard to accurately switch on a specific curve, we extend the optimal switching curve into a suboptimal switching zone. At the inside of the switching zone, the bang-bang suboptimal scheme is developed, which ensures that the system accurately reaches the desired target. Besides, inspired by the above mentioned PTOS, the linear control is also adopted when the system state error approaches zero.

The remainder of this paper is organized as follows: In Section 2, the problem is formulated. The time-optimal control is derived in Section 3. In Section 4, the proximate time-optimal control is developed. Section 5 analyzes the stability of the PTO. Numerical simulations are shown in Section 6. Finally, Section 7 concludes the paper.

2. PROBLEM FORMULATION

As shown in Fig. 1, assume that the velocity loop of the rigid body system features as a first-order link under an inner-loop controller, the system to be controlled is

$$\begin{cases} \dot{x}_1(t) = x_2(t) \\ \dot{x}_2(t) = -a \cdot x_2(t) + a \cdot u(t) \\ \boldsymbol{x}(0) = \boldsymbol{x}_0,\ \boldsymbol{x}(t_f) = \mathbf{0}, |u| \le \omega_m \end{cases} \tag{1}$$

where a indicates the system inner-loop bandwidth, ω_m indicates the system velocity saturation, u is the control input which represents the reference velocity. TOC is to find a control input $u^*(t)$, such that the system (1) can transfer from the initial state $\boldsymbol{x}_0$ to the zero point as quick as possible. The cost function is shown as

$$\min_u \ J = t_f \tag{2}$$

However, since direct application of the TOC to practical systems will lead to oscillations or even limit cycles, our goal is to develop a robust control law such that the closed-loop system makes a good compromise between dynamic response and steady-state precision.

3. TIME-OPTIMAL CONTROL

The Hamilton function of the system (1)∼(2) is written as

$$\begin{aligned} &H(\boldsymbol{x}(t), \boldsymbol{u}(t), \boldsymbol{\lambda}(t)) \\ &\quad = 1 + \lambda_1(t) \cdot x_2(t) + \lambda_2(t) \cdot (-a \cdot x_2(t) + a \cdot u(t)) \end{aligned} \tag{3}$$

where λ_1 and λ_2 are two co-states. According to the minimum principle, we need to derive u^* such that

$$H(\boldsymbol{x}^*, u^*, \boldsymbol{\lambda}) = \min_{|u| \le \omega_m} H(\boldsymbol{x}^*, u, \boldsymbol{\lambda}) \tag{4}$$

This is equivalent to

$$1 + \lambda_1 x_2^* - a\lambda_2 x_2^* + a\lambda_2 u^* \le 1 + \lambda_1 x_2^* - a\lambda_2 x_2^* + a\lambda_2 u \tag{5}$$

Therefore the optimal control input is given as

$$u^*(t) = -\mathrm{sgn}(\lambda_2) \cdot \omega_m \tag{6}$$

3.1 The Positive Maximum Control Input

When $u(t) = \omega_m$, the system states can be derived as

$$\begin{cases} x_1(t) = x_{10} + \omega_m t + \dfrac{1}{a}(x_{20} - \omega_m)\left(1 - e^{-at}\right) \\ x_2(t) = \omega_m + (x_{20} - \omega_m) e^{-at} \end{cases} \tag{7}$$

By eliminating t, the state trajectory is given as

$$a \cdot (x_1 - x_{10}) + (x_2 - x_{20}) + \omega_m \cdot \ln \frac{x_2 - \omega_m}{x_{20} - \omega_m} = 0 \tag{8}$$

This means that when $u(t) = \omega_m$, the system moves along the trajectory defined by (8) with initial state being (x_{10}, x_{20}). The switching curve is the one passing through the origin. By setting $(x_{10}, x_{20}) = (0, 0)$, we have

$$l_1 : a \cdot x_1 + x_2 + \omega_m \cdot \ln\left(1 - \frac{x_2}{\omega_m}\right) = 0 \tag{9}$$

Fig. 2 shows the state trajectories (8) (blue lines) with different (x_{10}, x_{20}) and the switching curve (9) (black lines). When $x_2 \le 0$ (black solid line), the system state lies in l_1 will move to the origin with the positive maximum control. But when $x_2 > 0$ (black dotted line), any system state lies in l_1 will run away from the origin with the positive maximum control input, which is not desired. Therefore, only the $x_2 < 0$ part is adopted as part of the final switching curve.

3.2 The Negative Maximum Control Input

Similar to the derivation of the positive maximum control input, the set of state trajectories in this case is given as

$$a \cdot (x_1 - x_{10}) + (x_2 - x_{20}) - \omega_m \cdot \ln \frac{x_2 + \omega_m}{x_{20} + \omega_m} = 0 \tag{10}$$

This means that when $u(t) = -\omega_m$, the system moves along the trajectory defined by (10) with initial state being (x_{10}, x_{20}). By setting $(x_{10}, x_{20}) = (0, 0)$, the switching curve is derived as

$$l_2 : a \cdot x_1 + x_2 - \omega_m \cdot \ln\left(1 + \frac{x_2}{\omega_m}\right) = 0 \tag{11}$$

Fig. 2 also shows the state trajectories (10) (blue lines) and the switching curve (11) (black lines). With the negative maximum control, l_2 values when $x_2 \ge 0$ (black solid line). Thus l_1 and l_2 complement each others' weakness, the whole switching curve $l_1 - o - l_2$ is formed.

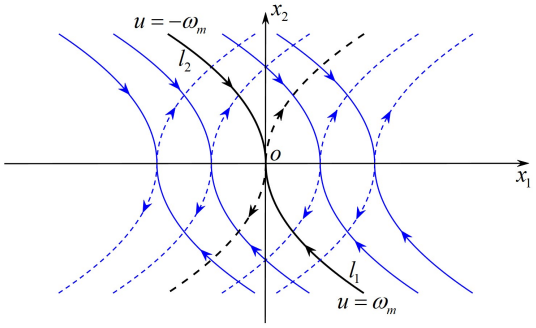

Fig. 2. The state trajectories with maximum control inputs

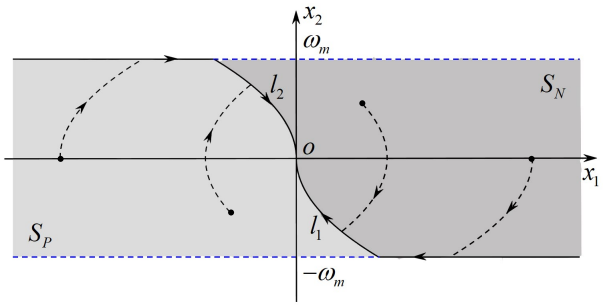

Fig. 3. The state trajectories when considering velocity saturation.

3.3 Saturation Consideration

In a practical system, we should take velocity saturation into consideration. According to (1), $|x_2| \leq \omega_m$. By considering this point, the trajectories in Fig. 3 reveal the change of system state under different initial values. The TOC input is:

$$u(t) = \begin{cases} \omega_m, & (x_1, x_2) \in S_P \cup l_1 \\ 0, & (x_1, x_2) = O \\ -\omega_m, & (x_1, x_2) \in S_N \cup l_2 \end{cases} \tag{12}$$

4. DEVELOPMENT OF PROXIMATE TIME-OPTIMAL CONTROL

The direct application of TOC to practical systems is not feasible due to the restriction of the sampling period, state measurement accuracy and so on. Oscillations or even limit cycles are possible to occur since the system is hard to match the single state in the switching curve. To address this problem, we attempt to extend the optimal switching curve into a suboptimal switching zone, which is easier to match. The principle of the switching zone is to ensure that a sampled system state will enter it, but not directly strides over. In the switching zone, the control input will switch to an suboptimal value which can drive the system moves to the origin. When the position x_1 is smaller than a certain threshold, the system enters the linear zone and linear control is adopted. The switching zone ensures the rapidity of the system, and also avoids oscillations and overshoots. The linear zone ensures a determinately local asymptotic stability and accurate stay at the origin.

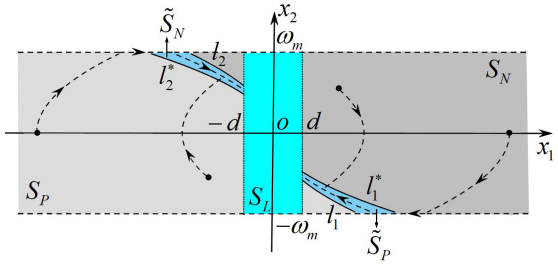

Fig. 4. The switching zone and linear zone for proximate time-optimal control.

Fig. 4 shows the switching zone and linear zone we are about to construct. The switching zone includes the region enclosed by l_1 and l_1^* ($\tilde{S}_P$) as well as l_2 and l_2^* ($\tilde{S}_N$). The linear zone is denoted by $|x_1| < d$ (S_L), where d is a boundary to be decided. The mathematical expressions of l_1^* and l_2^* will be developed according to the following rules:

① In the fourth quadrant: The boundary curve

$$l_1{}^* : a \cdot x_1 + x_2 + \omega_0 \cdot \ln\left(1 - \frac{x_2}{\omega_0}\right) = 0 \tag{13}$$

should ensure that when $u(t) = -\omega_m$, the next sample time state $(\tilde{x}_1, \tilde{x}_2)$ after (x_1^*, x_2^*) stays inside of the switching zone. Namely $(\tilde{x}_1, \tilde{x}_2)$ should stay above the curve l_1.

② In the second quadrant: The boundary curve

$$l_2{}^* : a \cdot x_1 + x_2 - \omega_0 \cdot \ln\left(1 + \frac{x_2}{\omega_0}\right) = 0 \tag{14}$$

should ensure that when $u(t) = \omega_m$, the next sample time state $(\tilde{x}_1, \tilde{x}_2)$ after (x_1^*, x_2^*) stays inside of the switching zone. Namely $(\tilde{x}_1, \tilde{x}_2)$ should stay below the curve l_2.

The deriving of l_1^* will be developed as follows. l_2^* is similar to that and will be omitted. According to the system state motion law (7), with $u(t) = \omega_m$ as the control input and $(x_1, x_2) \in l_1$ as the initial state, after a sampling period T, the state $(\tilde{x}_1, \tilde{x}_2)$ is

$$\begin{cases} \tilde{x}_1 = x_1 + \omega_m T + \dfrac{1}{a}(x_2 - \omega_m)\left(1 - e^{-aT}\right) \\ \tilde{x}_2 = x_2 \cdot e^{-aT} + \omega_m\left(1 - e^{-aT}\right) \end{cases} \tag{15}$$

which means

$$\begin{aligned} a \cdot \tilde{x}_1 + \tilde{x}_2 &= a x_1 + x_2 - a\omega_m T \\ &= -\omega_m \ln\left(1 - \frac{x_2}{\omega_m}\right) - a\omega_m T \end{aligned} \tag{16}$$

Since

$$x_2 = \left[\tilde{x}_2 - \omega_m\left(1 - e^{-aT}\right)\right] e^{aT} \tag{17}$$

Substituting (17) into (16), we have

$$\begin{aligned} & a \cdot \tilde{x}_1 + \tilde{x}_2 = \\ & = -\omega_m \ln\left(1 - \frac{\left(\tilde{x}_2 - \omega_m\left(1 - e^{-aT}\right)\right)}{\omega_m e^{-aT}}\right) - a\omega_m T \\ & = -\omega_m \ln\left(1 - \left(1 + \frac{\tilde{x}_2 - \omega_m}{\omega_m e^{-aT}}\right)\right) - a\omega_m T \\ & = -\omega_m \ln\left(e^{aT}\frac{\omega_m - \tilde{x}_2}{\omega_m}\right) - a\omega_m T \\ & = -\omega_m\left(aT + \ln\left(1 - \frac{\tilde{x}_2}{\omega_m}\right)\right) - a\omega_m T \\ & = -\omega_m \ln\left(1 - \frac{\tilde{x}_2}{\omega_m}\right) - 2a\omega_m T \end{aligned} \tag{18}$$

This means the trajectory formed by $(\tilde{x}_1, \tilde{x}_2)$ is

$$\tilde{l}_1 : a \cdot \tilde{x}_1 + \tilde{x}_2 + \omega_m \ln\left(1 - \frac{\tilde{x}_2}{\omega_m}\right) = -2a\omega_m T \tag{19}$$

Fig. 5 shows the relationship among l_1, l_1^*, and $\tilde{l}_1$. There must exists an intersection $(\tilde{x}_{10}, \tilde{x}_{20})$ between l_1^* and $\tilde{l}_1$. The area to the left of the intersection is selected as the linear zone because $\tilde{l}_1$ lies above l_1^*. By setting $\tilde{x}_{10} = d$ and substitute it into (19), we have

$$\begin{aligned} & a \cdot \tilde{x}_{10} + \tilde{x}_{20} + \omega_m \ln\left(1 - \frac{\tilde{x}_2}{\omega_m}\right) = -2a\omega_m T \\ & \Rightarrow \ln\left(1 - \frac{\tilde{x}_{20}}{\omega_m}\right) - \left(-\frac{\tilde{x}_{20}}{\omega_m} - \left(\frac{a\tilde{x}_{10}}{\omega_m} + 2aT\right)\right) = 0 \end{aligned} \tag{20}$$

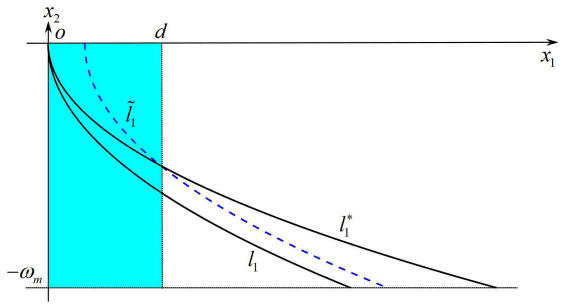

Fig. 5. The relationship among l_1, l_1^*, and $\tilde{l}_1$.

By defining

$$y = \frac{-\tilde{x}_{20}}{\omega_m}, \quad b_0 = \frac{a\tilde{x}_{10}}{\omega_m} + 2aT \tag{21}$$

Equation (20) can be expressed as

$$f(y) = \ln(1+y) - (y - b_0) = 0 \tag{22}$$

The analytic solution of (22) is difficult to be obtained. Therefore, the simple bisection algorithm can be used to derive the numerical solution. Once we get the solution y^*, $\tilde{x}_{20}$ is

$$\tilde{x}_{20} = -y^* \cdot \omega_m \tag{23}$$

Thus the intersection $(\tilde{x}_{10}, \tilde{x}_{20})$ is derived. Now, the intersection is used to derive the boundary curve l_1^*. By substituting $(\tilde{x}_{10}, \tilde{x}_{20})$ into (13), we have

$$\begin{aligned} &a \cdot \tilde{x}_{10} + \tilde{x}_{20} + \omega_0 \cdot \ln\left(1 - \frac{\tilde{x}_{20}}{\omega_0}\right) = 0 \\ &\Rightarrow \ln\left(1 - \frac{\tilde{x}_{20}}{\omega_0}\right) - \left(1 + \frac{a\tilde{x}_{10}}{\tilde{x}_{20}}\right) \cdot \left(-\frac{\tilde{x}_{20}}{\omega_0}\right) = 0 \end{aligned} \tag{24}$$

By defining

$$k = \left(1 + \frac{a\tilde{x}_{10}}{\tilde{x}_{20}}\right), \quad z = -\frac{\tilde{x}_{20}}{\omega_0} \tag{25}$$

Equation (24) can be expressed as

$$f(z) = \ln(1+z) - k \cdot z = 0 \tag{26}$$

Similarly, the bisection algorithm can be used to derive the numerical solution of (26). With the derived z^*, ω_0 is

$$\omega_0 = -\frac{\tilde{x}_{20}}{z^*} \tag{27}$$

Thus the boundary curve l_1^* is obtained, the switching zone is now constructed.

To ensure any state within the switching zone enters the linear zone, we derive a control input $u(t) = \omega_c \in [\omega_0, \omega_m]$ such that the system moves along the trajectory:

$$a \cdot x_1 + x_2 + \omega_c \cdot \ln\left(1 - \frac{x_2}{\omega_c}\right) = 0 \tag{28}$$

Rewrite (28) as

$$\ln\left(1 - \frac{x_2}{\omega_c}\right) = -\frac{ax_1 + x_2}{\omega_c} = \left(1 + \frac{ax_1}{x_2}\right) \cdot \left(-\frac{x_2}{\omega_c}\right) \tag{29}$$

Similarly, by defining

$$k = 1 + \frac{ax_1}{x_2}, \quad w = -\frac{x_2}{\omega_c} \tag{30}$$

Equation (30) can be expressed as

$$f(w) = \ln(1+w) - k \cdot w = 0 \tag{31}$$

Also using the bisection algorithm, the control input is derived as

$$\omega_c = -\frac{x_2}{w^*} \tag{32}$$

The above analysis aims at the fourth quadrant. For the second quadrant, the results can be easily derived because of symmetry. For the system state inside of the switching zone enclosed by l_2 and l_2^* ($\tilde{S}_N$), the control input $u(t) = -\omega_c \in [-\omega_m, -\omega_0]$ is similarly derived according to the trajectory

$$a \cdot x_1 + x_2 - \omega_c \cdot \ln\left(1 + \frac{x_2}{\omega_c}\right) = 0 \tag{33}$$

The details are omitted here. With the control input $u(t) = -\omega_c$, the system state inside of the switching zone enclosed by l_2 and l_2^* will move along the trajectory (33).

The last thing needs to be concerned is the linear zone. The threshold d should be determined by different performance requirements. The control input of the linear zone is

$$u(t) = -k_1 \cdot x_1 - k_2 \cdot x_2 \tag{34}$$

where k_1 and k_2 are two adjustable parameters.

As a whole, the compound PTO control law is

$$u(t) = \begin{cases} \omega_m, & (x_1, x_2) \in S_P \cup l_1 \\ -\omega_c \cdots (33), & (x_1, x_2) \in \tilde{S}_N \cup l_2^* \\ \text{PD} \cdots (34), & (x_1, x_2) \in S_L \\ 0, & (x_1, x_2) = O \\ \omega_c \cdots (28), & (x_1, x_2) \in \tilde{S}_P \cup l_1^* \\ -\omega_m, & (x_1, x_2) \in S_N \cup l_2 \end{cases} \tag{35}$$

We call control inputs in the regions S_N and S_P as the bang-bang optimal schemes, control inputs in the regions $\tilde{S}_N$ and $\tilde{S}_P$ as the bang-bang suboptimal schemes, and control input in the region S_L as the linear scheme.

5. STABILITY ANALYSIS

The PTO control involves two switches, one is from the bang-bang optimal scheme to the bang-bang suboptimal scheme, and the other is from the bang-bang suboptimal scheme to the linear scheme. Take the fourth quadrant as the example, stability analysis is shown as follows.

Fig. 6 shows the system trajectory evolution when initial state lies in the fourth quadrant. With $u(t) = -\omega_m$, the system crosses over the curve l_1^* and enters the switching zone. Because the boundary cure l_1^* lies above $\tilde{l}_1$ when $|x_1| > d$, once the system state enters the switching zone, it must satisfy

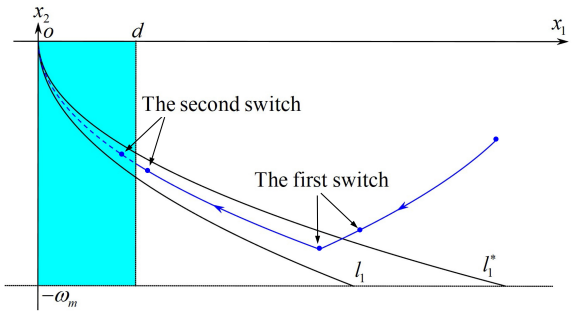

Fig. 6. The trajectory evolution when initial state lies in the fourth quadrant.

$$\begin{cases} a \cdot x_1 + x_2 + \omega_m \cdot \ln\left(1 - \dfrac{x_2}{\omega_m}\right) \geq 0 \\ a \cdot x_1 + x_2 + \omega_0 \cdot \ln\left(1 - \dfrac{x_2}{\omega_0}\right) \leq 0 \end{cases} \tag{36}$$

Equation (36) means that the system will stay in the switching zone at a certain sampling time. In the switching zone, the control input switches to $u(t) = \omega_c \in [\omega_0, \omega_m]$. As the blue curve shown in Fig. 6, the system moves along the trajectory (28), and enters the linear zone at last.

In the linear zone, the closed-loop system performs as

$$\begin{cases} \dot{x}_1 = x_2 \\ \dot{x}_2 = -ak_1 x_1 - a(1 + k_2) x_2 \end{cases} \tag{37}$$

By setting the Lyapunov candidate as

$$V(x_1, x_2) = ak_1 \cdot x_1^2 + x_2^2 \tag{38}$$

We have

$$\begin{aligned} \dot{V} &= 2ak_1 x_1 x_2 + 2x_2 \left[-ak_1 x_1 - a(1 + k_2) x_2\right] \\ &= -2a(1 + k_2) x_2^2 \end{aligned} \tag{39}$$

Thus $V > 0$ and $\dot{V} \leq 0$ if $1 + k_2 > 0$, $k_1 > 0$. Since $x_2 = 0 \Rightarrow x_1 = 0$, the system is local asymptotically stable. Therefore, the whole system is stable with the developed PTO control law.

6. NUMERICAL SIMULATION

In this section, numerical simulations are conducted among the PTO, TO, and PD controllers to compare their performances. Assume that the velocity loop bandwidth is 30Hz and rated speed is 300mm/s, the position range is ±50mm. With a 2ms sampling period, the step signal, ramp signal and sinusoidal signal are tested in following subsections. The parameters of controllers are carefully adjusted by the Ziegler-Nichols method. In the PD controller, $k_p = 356$ and $k_d = 1.15$. In the TO controller, the maximum control input is set as the rated speed 300mm/s. In the PTO controller, the boundary of linear zone is set as the 1% of the position range, namely 0.5mm. And in its linear zone, $k_1 = 323$ and $k_2 = 3.6$.

6.1 Step Command Signal

A 5mm step signal, which is 10% of the position range, is commanded in this case. Fig. 7 shows the system responses with the TO, PD, and PTO controllers. With the TO controller, it can be seen that there exist persistent oscillations in the steady-state phase. This phenomenon is eliminated by the PD controller, but with the same overshoot, it takes 31% more adjustment time than the PTO. The PTO controller combines the advantages of both controllers, it features with a more stable steady-state phase compared with the TO controller and a quicker dynamic process compared with the PD controller. The trajectories of system control error shown in Fig. 8 also confirm this point.

6.2 Ramp Command Signal

A ramp signal, which linearly increases from 0 to 30mm with a slope of 200mm/s, is commanded in this case. Figs. 9 and 10 show the system position and velocity responses. And Fig. 11 shows the system control error

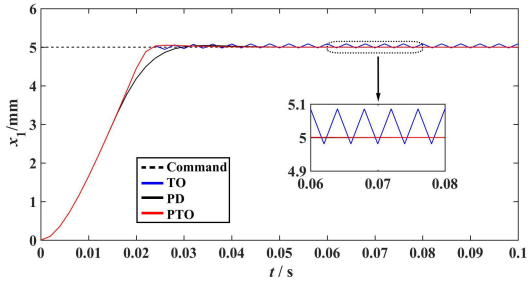

Fig. 7. The position responses under step signal.

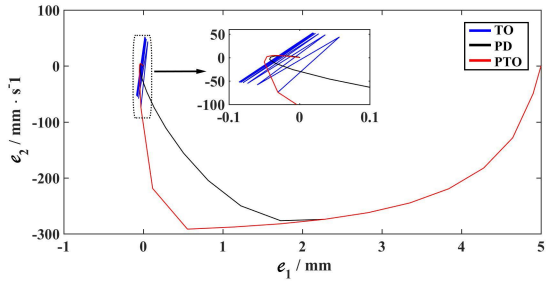

Fig. 8. The state error trajectories under step signal.

trajectories. Similarly, it can be seen that there also exist series position and velocity oscillations with the TO controller. And the PD controller delays a large value about the command signal. The developed PTO controller makes a good compromise between dynamic and steady-state characteristics: the command signal is tracked smoothly in a short time, and the state error trajectory reaches zero without any oscillation.

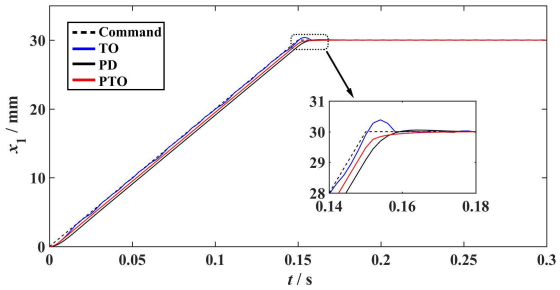

Fig. 9. The position responses under ramp signal.

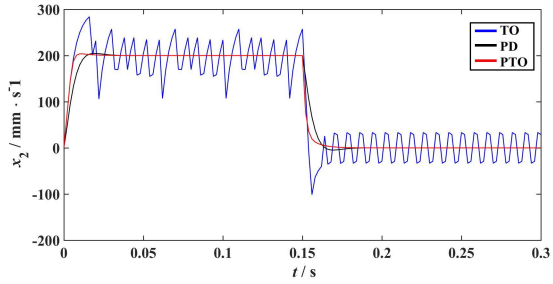

Fig. 10. The velocity responses under ramp signal.

6.3 Sinusoidal Command Signal

A sinusoidal signal, with a magnitude of 5mm and a frequency of 5Hz, is commanded in this case. Figs. 12 and 13 show the system position and velocity responses.

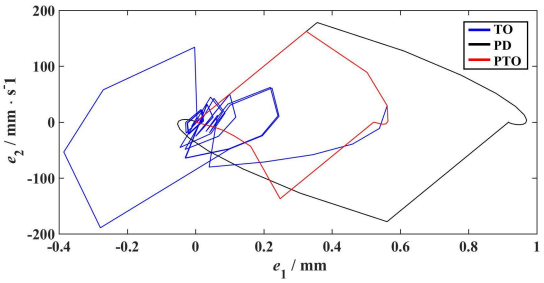

Fig. 11. The state error trajectories under ramp signal.

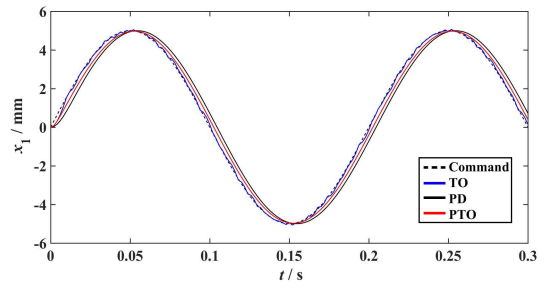

Fig. 12. The position responses under sinusoidal signal.

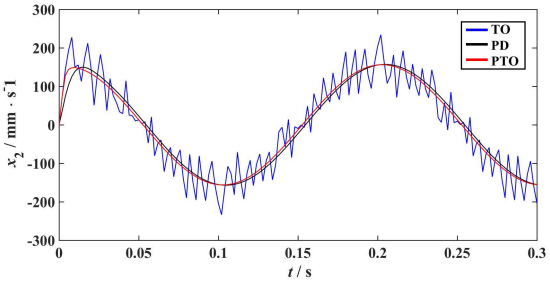

Fig. 13. The velocity responses under sinusoidal signal.

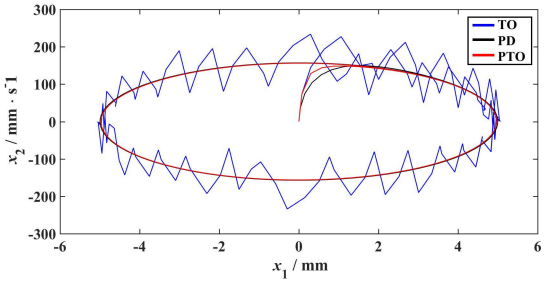

Fig. 14. The state trajectories under sinusoidal signal.

And Fig. 14 shows the system state trajectories, which indicate that the system with the TO controller is much fluctuant than that with the PD and PTO controllers. With the TO controller, there is basically no phase delay but oscillations exist. With the PTO controller, the phase delay is about 4.5°, which is only 55.5% of the phase delay with the PD controller (about 8.1°).

7. CONCLUSION

This paper focuses on the proximate time-optimal control for rigid body systems, whose velocity dynamics are assumed as a first-order inertial link under the inner-loop controller. The optimal switching curves are extended into a suboptimal switching zone. The goal is to ensure that a sampled state will stay in this zone, but not directly strides over. At the inside of the switching zone, the bang-bang suboptimal scheme is developed. When the position signal is smaller than a certain threshold, the system enters the linear zone and the linear scheme is adopted. The numerical simulations indicate the advantages of our work: Compared with the TO, our PTO avoids oscillations and overshoots. And compared with the PD, our PTO has a shorter adjustment time and a quicker dynamic response.

REFERENCES

Bertsekas, D.P. (1995). *Dynamic programming and optimal control*, volume 1. Athena scientific Belmont, MA.

Bonifacius, L., Pieper, K., and Vexler, B. (2019). Error estimates for space-time discretization of parabolic time-optimal control problems with bang-bang controls. *SIAM Journal on Control and Optimization*, 57(3), 1730–1756.

Braker, R.A. and Pao, L.Y. (2017). Proximate time-optimal control of a harmonic oscillator. *IEEE Transactions on Automatic Control*, 63(6), 1676–1691.

Bryson, A.E. (2018). *Applied optimal control: optimization, estimation and control*. Routledge.

Choi, Y.M., Jeong, J., and Gweon, D.G. (2006). A novel damping scheduling scheme for proximate time optimal servomechanisms in hard disk drives. *IEEE transactions on magnetics*, 42(3), 468–472.

Dhanda, A. and Franklin, G.F. (2009). An improved 2-dof proximate time optimal servomechanism. *IEEE Transactions on magnetics*, 45(5), 2151–2164.

Featherstone, R. (2014). *Rigid body dynamics algorithms*. Springer.

Grimholt, C. and Skogestad, S. (2016). Optimal pid control of double integrating processes. *IFAC-PapersOnLine*, 49(7), 127–132.

Herlant, L.V., Holladay, R.M., and Srinivasa, S.S. (2016). Assistive teleoperation of robot arms via automatic time-optimal mode switching. In *The 11th ACM/IEEE International Conference on Human Robot Interaction*, 35–42. IEEE.

HU, Y., TENG, Z., and CHENG, G. (2018). Expanded proximate time-optimal servo control and its experimental verification. *Electric Machines & Control Application*, 45(9), 59–64.

Lu, Y.S. and Shieh, R. (2014). A jerk-constrained time-optimal servo with disturbance compensation. *Control Engineering Practice*, 28, 49–57.

Park, M.H. and Won, C.Y. (1991). Time optimal control for induction motor servo system. *IEEE Transactions on Power Electronics*, 6(3), 514–524.

Rao, V.G. and Bernstein, D.S. (2001). Naive control of the double integrator. *IEEE Control Systems Magazine*, 21(5), 86–97.

Workman, M.L., Kosut, R.L., and Franklin, G.F. (1987a). Adaptive proximate time-optimal servomechanisms: Continuous time case. In *1987 American Control Conference*, 589–594. IEEE.

Workman, M.L., Kosut, R.L., and Franklin, G.F. (1987b). Adaptive proximate time-optimal servomechanisms: Discrete-time case. In *26th IEEE Conference on Decision and Control*, volume 26, 1548–1553. IEEE.